Available online at www.sciencedirect.com
ScienceDirect
Journal of Magnetism and Magnetic Materials 320 (2008) 354–363
Journal of magnetism and magnetic materials
www.elsevier.com/locate/jmmm

Precise measurements of radio-frequency magnetic susceptibility in ferromagnetic and antiferromagnetic materials

M.D. Vannette[a], A.S. Sefat[a], S. Jia[a], S.A. Law[a], G. Lapertot[b], S.L. Bud'ko[a], P.C. Canfield[a], J. Schmalian[a], R. Prozorov[a,*]

[a]*Ames Laboratory and Department of Physics and Astronomy, Iowa State University, Ames, IA 50011, USA*
[b]*Departement de Recherche Fondamentale sur la Mati'ere Condensee, SPSMS, CEA Grenoble, 38054 Grenoble, France*

Received 6 May 2007; received in revised form 18 June 2007
Available online 29 June 2007

Abstract

Dynamic magnetic susceptibility, χ, was studied in several intermetallic materials exhibiting ferromagnetic, antiferromagnetic and metamagnetic transitions. Precise measurements by using a 14 MHz tunnel diode oscillator (TDO) allow detailed insight into the field and temperature dependence of χ. In particular, local moment ferromagnets show a sharp peak in $\chi(T)$ near the Curie temperature, T_C. The peak amplitude decreases and shifts to higher temperatures with very small applied dc fields. Anisotropic measurements of $CeVSb_3$ show that this peak is present provided the magnetic easy axis is aligned with the excitation field. In a striking contrast, small moment, itinerant ferromagnets (i.e., $ZrZn_2$) show a broad maximum in $\chi(T)$ that responds differently to applied field. We believe that TDO measurements provide a very sensitive way to distinguish between local and itinerant moment magnetic orders. Local moment antiferromagnets do not show a peak at the Néel temperature, T_N, but only a sharp decrease of χ below T_N due to the loss of spin-disorder scattering changing the penetration depth of the ac excitation field. Furthermore, we show that the TDO is capable of detecting changes in spin order as well as metamagnetic transitions. Finally, critical scaling of $\chi(T,H)$ in the vicinity of T_C is discussed in $CeVSb_3$ and $CeAgSb_2$.

PACS: 75.30.Kz; 75.40.Gb

Keywords: Dynamic magnetic susceptibility; Magnetic transitions; Critical scaling

1. Introduction

Dynamic magnetic susceptibility, $\chi = \partial M/\partial H$, is an important quantity to measure in magnetic materials. It couples directly to the spin structure in the ordered state, critical fluctuations near the transition, and the magnetic polarizability of the conduction electrons. The sensitivity of techniques for measuring dynamic susceptibility varies significantly with frequency and with the way the signal is obtained. Amplitude- domain measurements with lock-in amplifiers operate at relatively low frequencies and are prone to waveform distortions and phase drift. Frequency-domain measurements are much more sensitive, but require high-Q circuits and frequency scanning to find the resonance frequency. The most sensitive probes utilize microwave cavity perturbation at typical frequencies of $f \geqslant 1$–100 GHz. However, at these frequencies, nonlinear magnetic effects as well as the anomalous skin effect may be of importance and interpretation of the results becomes difficult.

Tunnel diode oscillators (TDO) are well suited to fill the spectral gap between these two extremes since they can be tuned to operate in the radio-frequency (rf) range, as was suggested by Clover and Wolf [1]. A TDO is essentially a self-resonating LC tank circuit biased by a tunnel diode. A properly constructed circuit allows one to measure changes in the magnetic moment on the order of a 10^{-12} emu. In addition, the excitation field is very small, of the order of 20 mOe, which is very useful in cases of highly nonlinear

*Corresponding author. Tel.: +1 515 294 9901.
E-mail address: prozorov@ameslab.gov (R. Prozorov).

0304-8853/$ - see front matter © 2007 Elsevier B.V. All rights reserved.
doi:10.1016/j.jmmm.2007.06.018

and/or hysteretic samples. These facts taken together suggest using this instrument to measure magnetic susceptibility in the vicinity of magnetic transitions where critical fluctuations are of importance, but may be easily suppressed by fields of only a few oersted (typical for conventional magnetometry). The major development of the TDO as an instrument was reported by Van Degrift in 1975 [2], primarily to measure dielectric constants of various materials. Earlier in that same year, Habbal et al. described a simple TDO setup that could be used to measure the rf susceptibility of samples over a broad temperature range [3]. More recently, TDO's have been developed to measure minute changes in the London penetration depth of small superconducting samples [4]. In addition, the technique is sensitive enough to measure quantum oscillations in resistivity via the normal skin depth [5].

Several groups have used TDO's to detect the ferromagnetic (FM) transition [6–8], however there has been little attention paid to the vicinity of the transition itself. In this paper we demonstrate that the TDO is a versatile and extremely sensitive quantitative probe of FM, antiferromagnetic (AFM), and metamagnetic (MM) transitions. This sensitivity proves particularly important when dealing with questions related to small and very field-dependent features associated with the critical fluctuations and delocalized magnetic moment of conduction electrons.

2. Experimental

2.1. Samples

Single crystals of several intermetallic systems were used throughout this study. All samples, except for $ZrZn_2$, were grown via high-temperature solution growth [9,10]. CeSb was grown out of tin flux [11] while $CeVSb_3$ was grown out of excess Sb [12]. [Ce, Sm]$AgSb_2$ were grown out of excess Sb and Ag [14,13]. $GdFe_2Zn_{20}$ was grown out of excess Zn [15]. $ZrZn_2$ was grown from a melt of $ZrZn_{2.006}$ to compensate for zinc lost due to vaporization as described in Ref. [16]. Samples for TDO measurements were either cut with a blade or used as grown and mounted on a 1 mm diameter by 15 mm long sapphire rod. The TDO circuit and sample were enclosed in a vacuum can and placed in the bore of a superconducting magnet with field range of 0–90 kOe. The axis of the excitation coil and the static field were aligned. Both of the [Ce, Sm]$AgSb_2$ samples were plates of dimensions $0.75 \times 0.75 \times 0.2$ mm with the c-axis perpendicular to the face. In these samples the c-axis was also aligned with the coil axis. The CeSb sample was a rectangular slab with dimensions of $0.25 \times 0.25 \times 0.5$ mm, the long axis aligned with the [1 0 0] axis as well as with the coil axis. The Ce_3Al_{11} and $CeVSb_3$ samples were tapered needles with lengths of 1 mm. The aluminum compound had a square base approximately 0.4 mm on a side, while the triantimonide had a rectangular base approximately 0.4×0.1 mm. In both of these samples the long axis coincided with the magnetic easy axis as well as the coil axis. A small piece of $CeVSb_3$ was cut from the original sample in order to study the anisotropic response. This piece had dimensions of $0.5 \times 0.2 \times 0.1$ mm with the 0.2 mm dimension aligned with the c-axis as determined from Laue diffraction measurements. The $ZrZn_2$ sample was roughly cubic with an edge length of 0.5 mm. The low anisotropy of this compound eliminated the need to align any particular axis with the coil. $GdFe_2Zn_{20}$ was a triangular prism. The base was approximately 0.2×0.2 mm and the length was approximately 0.5 mm. As with $ZrZn_2$, the low anisotropy of $GdFe_2Zn_{20}$ eliminated the need for a particular crystal axis alignment. The long axis was aligned with the coil. Samples used in magnetization and conventional resistivity measurements were taken from the same growths as those used in the TDO experiments. Magnetization measurements were performed in a *quantum design* MPMS operating down to 1.8 K with maximum applied field of 55 kOe. Specific heat and conventional four-probe transport measurements were performed in a quantum design PPMS system operating down to 1.8 K with a 90 kOe superconducting magnet.

The compounds chosen for this study span the range from well defined, local moment ferromagnetism ($CeVSb_3$, $CeAgSb_2$) to small moment, itinerant ferromagnetism ($ZrZn_2$), to $GdFe_2Zn_{20}$, a compound that apparently combines local moment (Gd-based) ferromagnetism with a near itinerant, band component. In addition Ce_3Al_{11} and CeSb were studied as examples of multiple, temperature and field dependent transitions in local moment systems. Whereas each of these compounds are interesting in their own right [5,11,12,15–18] they are being used in this study as bench marks.

2.2. Principle of TDO operation

The main component of a TDO is a tunnel diode. It has a heavily overdoped, narrow (~100 Å), p–n junction, so that valence of p-side and conduction of n-side bands overlap. Above certain bias voltage, forward bias results in a lesser overlap of the two bands, thus reducing the tunneling current. As a result, the device exhibits a bias region with negative differential resistance. When biased to this voltage region, the diode can be used to drive the tank circuit resulting in a self-resonating LC oscillator. The frequency is always at the resonance, which is the main advantage of this device. Careful design and good thermal stability result in a circuit that resonates in the rf range with a stability of 0.05 Hz over hours to days [19,20]. We report results obtained with a TDO mounted in a ^{3}He cryostat with a temperature range from 0.3–150 K operating at a frequency of approximately 14 MHz. A dc external field up to 90 kOe can be applied to study field-dependent properties. A sample is placed in a coil which acts as the inductor in the LC tank circuit. The shift of the resonant frequency is directly related to the dynamic susceptibility, χ, of the sample.

The frequency of oscillation for an inductor–capacitor circuit with inductance L and capacitance C is given by

$$f_0 = \frac{1}{2\pi\sqrt{LC}}. \quad (1)$$

If the inductance changes a small amount to $L + \Delta L$ the new frequency can be written as

$$f_0 + \Delta f = \frac{1}{2\pi\sqrt{(L+\Delta L)C}}. \quad (2)$$

Expanding this expression for small values of ΔL gives, to first order,

$$\Delta f \approx -\frac{1}{2}\frac{\Delta L}{L} f_0. \quad (3)$$

If a magnetically active sample is responsible for the change in inductance, one can rewrite the above expression as

$$\frac{\Delta f}{f_0} \approx -\frac{1}{2}\frac{V_s}{V_c} 4\pi\chi_m, \quad (4)$$

where χ_m is the measured susceptibility, V_s is the sample volume, and V_c is the inductor (or coil) volume. In the above expression, f_0 corresponds to the empty coil resonant frequency and Δf is the shift in resonance caused by inserting the sample.

If there is non-zero demagnetization factor, N, measured susceptibility, χ_m, is related to the true (zero-demagnetization) susceptibility, χ_t, via

$$\chi_m = \frac{\chi_t}{1 + 4\pi N\chi_t}. \quad (5)$$

Thus, the change in resonant frequency is directly proportional to the dynamic magnetic susceptibility of any sample placed in the coil. An increase in magnetic susceptibility results in a decrease in resonant frequency and *vice versa* for a diamagnetic response. In practice, we measure the difference (df) between the resonant frequency (f_{res}) and a local oscillator (f_{LO}). The local oscillator frequency is set higher than the resonance, so a decrease in f_{res} results in an increase in df. Hence, the raw data directly correspond to the susceptibility of the sample. Since we record changes in this difference (Δ df), we set the highest temperature of any data set (common to all runs in that set) to zero.

Measured susceptibility, χ_m, is composed of two parts: (1) the magnetic response of the bulk to an applied field and (2) the screening due to the skin effect in metals. The two effects add to give the total χ.

$$\chi_{total} = \chi_{mag} + \chi_{skin}. \quad (6)$$

The usual interpretation of χ_{mag} comes from $M = \chi_{mag} H$. This may be paramagnetic or diamagnetic. χ_{skin} is always diamagnetic. In normal metals this is conventional skin depth, whereas in superconductors this contribution is associated with London penetration depth. For conducting ellipsoidal samples χ_{skin} can be written as

$$\chi_{skin} = -\frac{1}{4\pi}\left(1 - \frac{\delta}{2R}\tanh\frac{2R}{\delta}\right). \quad (7)$$

Here R is the characteristic dimension of the sample perpendicular to the axis of the coil and δ is the skin depth [21]. Skin depth is related to resistivity, ρ as below

$$\delta = \sqrt{\frac{2\rho}{\mu f}}, \quad (8)$$

where f is the oscillator frequency and μ is the magnetic permeability of the material [22]. If R is much larger than δ then Eq. (7) may be written as

$$\chi_{skin} = -\frac{1}{4\pi}\left(1 - \frac{\delta}{2R}\right). \quad (9)$$

If necessary, conventional resistivity measurements can be made and the effect of diamagnetic screening can be subtracted. While some of our samples do show a change in resistivity, in the vicinity of a ferromagnetic phase transition the dominant contribution comes from the magnetic component. Further, over the field range of interest in the vicinity of the phase transition (typically less than 1 kOe) for the samples presented here magnetoresistance is negligible. Therefore, we can also subtract a "high" field data run if we need to eliminate the skin-depth background.

3. Results

3.1. Probing magnetic transitions

The materials $CeVSb_3$, $CeAgSb_2$, $ZrZn_2$, and $GdFe_2Zn_{20}$ exhibit ferromagnetic order at approximately 4.5, 9.8, 28, and 86 K, respectively. $SmAgSb_2$ is an antiferromagnet with a Néel temperature of approximately 10 K. $CeVSb_3$ and $CeAgSb_2$ are local moment magnets with a reported saturated moments of 1.80 μ_B [12] and 0.4 μ_B [14] per cerium atom. $ZrZn_2$ is a weak itinerant ferromagnet which is also highly unsaturated, showing a large relative increase in moment up to fields of 5.5 T. Its reported ordered moment is about 0.17 μ_B per formula unit [18]. The ground state of $GdFe_2Zn_{20}$ is reported as a mixed Gd-local moment/Fe-itinerant system with an unusually high T_C attributed to a highly polarizable conduction electron background. DC magnetization measurements show that it carries a moment of about 6.5 μ_B per formula unit with an induced Fe moment opposite the Gd [15]. We present measured χ for each material in several low fields.

3.1.1. $CeVSb_3$

The ternary rare earth compound $CeVSb_3$ undergoes a ferromagnetic transition at 4.5 K with moments aligned along the crystallographic c-axis [12]. The material grows as elongated plates and fractures into needles with the long axis along the ferromagnetic easy axis. Fig. 1 shows the

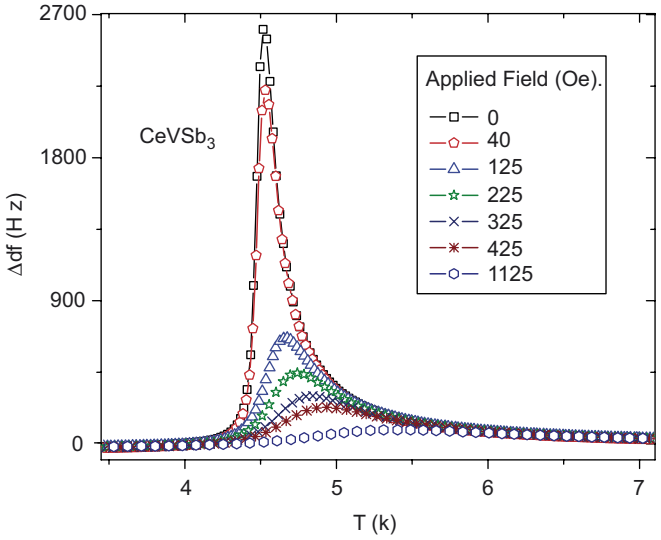

Fig. 1. (Color online) Change in resonant frequency passing through the ferromagnetic transition of $CeVSb_3$ in various dc magnetic fields. The peak amplitude monotonically decreases as field is increased.

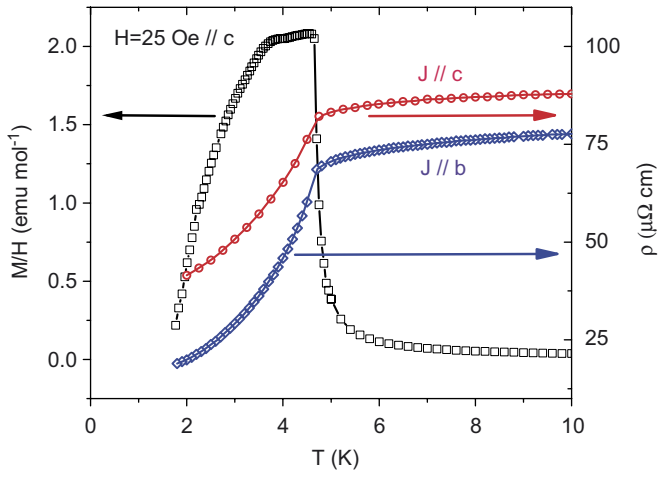

Fig. 2. (Color online) Zero field cooled static M/H (left axis) and resistivity (right axis) along easy-axis (J//c) and in plane (J//b) for $CeVSb_3$ near T_C.

resonator frequency shift relative to the high-temperature value as temperature was increased from 3.5 to 7 K in several applied magnetic fields. The zero field response is quite sharp and very large. A field of 125 Oe is sufficient to suppress the susceptibility peak by 70%. A 1 kOe field almost completely suppresses the peak, and shifts it to above 5 K. Similar behavior has been reported for an amorphous Fe–Ni–B–Si alloy using a compensated coil ac susceptometer [23,24] operating at 231 Hz, but the zero field data shown here have a much sharper response.

Fig. 2 shows the low field, easy axis magnetization and the resistivity measured in two in-plane directions: along the magnetic easy axis and perpendicular to it. The perpendicular resistivity corresponds to a skin depth ranging from 134 μm just above T_C to 67 μm at 2 K for our operating frequency. The dimensions perpendicular to

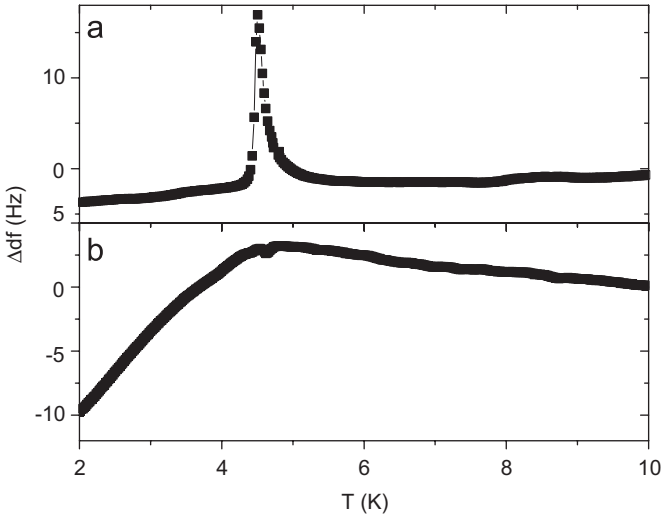

Fig. 3. Anisotropic zero field response of the TDO to $CeVSb_3$. Panel (a) shows the response with the magnetic easy axis aligned with the excitation field. Panel (b) shows the response with the magnetic easy axis perpendicular to the excitation field. These measurements were performed on a small piece of the original sample. The much smaller signal amplitude when compared with Fig. 1 is due to the smaller sample size.

the excitation field of the sample used were approximately 400 × 100 μm at the widest point. This means the TDO data are relatively insensitive to changes in resistivity because over the whole range the skin depth is greater than or of the order of the size of the sample. This explains the relatively flat response far from the ordering temperature.

Fig. 3 shows the zero field anisotropic response of the TDO to a small piece of $CeVSb_3$ cut from the original sample. When the magnetic easy axis is aligned with the excitation field (H_{exc}) there is the sharp peak in susceptibility. However, when the H_{exc} is perpendicular to the easy axis no peak is present. From measurements on $CeAgSb_2$ it is unlikely that the different responses in the different orientations is due to demagnetization effects. The $CeAgSb_2$ data show similar responses separately for the FM axis aligned with and perpendicular to the excitation field (see below). We do see anisotropic response, and this will be studied further.

Fig. 4 shows the TDO response and specific heat measurement in zero field in the vicinity of the phase transition. The TDO peak lies within the specific heat peak. The latter peak is often taken as a demarcation of the critical fluctuation region. This suggests that critical scaling analysis may be applicable. Such analysis is presented in the discussion.

3.1.2. [Ce, Sm]$AgSb_2$

Fig. 5 shows the zero field frequency shift of the resonator in response to [Ce, Sm]$AgSb_2$. The cerium compound orders with a ferromagnetic component along the *c*-axis at 9.8 K, whereas the samarium compound orders antiferromagnetically at 10 K [14]. Both samples show a decrease in resistivity due to the loss of spin disorder scattering, but the effect is much more pronounced in

the cerium compound (note different scales in figure). Since the samples have the same dimensions, the most likely explanation of the differences in the resistivity components is from the different changes in ρ that occur for each compound. $CeAgSb_2$ has a resistivity of approximately 90 μΩ cm at 11 K which drops to about 1.2 μΩ cm at approximately 2 K. $SmAgSb_2$ has a resistivity of about 1 μΩ cm at 11 K which drops to about 0.5 μΩ cm at 2 K [14]. Since we directly probe changes in sample properties (χ and ρ) versus temperature, the larger change in diamagnetic screening in the Ce compound manifests itself as a larger shift in the resonant frequency of the circuit. Further, the FM ordering of the cerium moments is accompanied by a sharp peak in the resonator response. This peak is absent in the AFM $SmAgSb_2$. Fig. 6 compares the zero field TDO responses of the cerium compound in two orientations relative to H_{exc}. It is seen that with the FM easy axis aligned with the excitation field, the susceptibility peaks at the Curie temperature. However, the in-plane susceptibility shows no such peak. As discussed above, the different demagnetization factors along the magnetic easy axes of $CeAgSb_2$ (high value) and $CeVSb_3$ (low value) do not

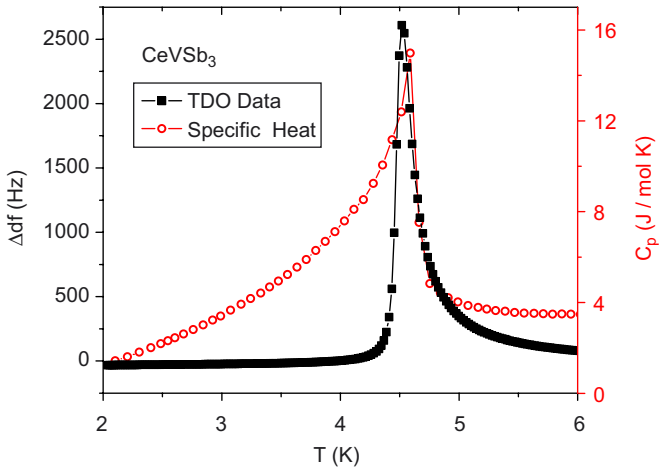

Fig. 4. (Color online) Comparison of zero field TDO data (left axis) with specific heat (right axis) for $CeVSb_3$. Solid squares are TDO data and open circles are specific heat.

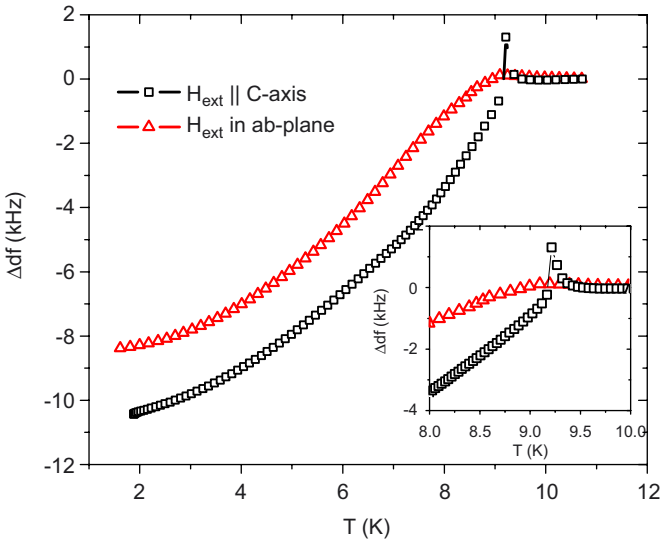

Fig. 6. (Color online) Anisotropic response of the TDO to $CeAgSb_2$. Squares correspond to the c-axis aligned with the excitation field. Circles correspond to the excitation field lying in plane. Some data points are omitted for clarity.

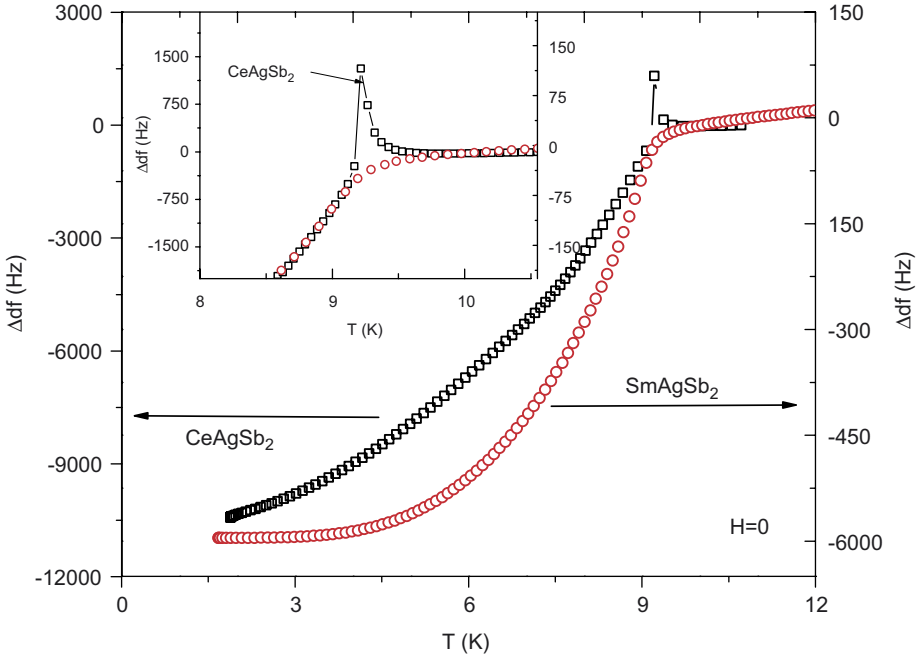

Fig. 5. (Color online) Change in resonant frequency as temperature is varied through the ferromagnetic transition of $CeAgSb_2$ and the antiferromagnetic transition of $SmAgSb_2$. The sharp peak is associated with $CeAgSb_2$. Note both systems exhibit a decrease in resistivity due to loss of spin disorder. Inset is a detail of the transitions.

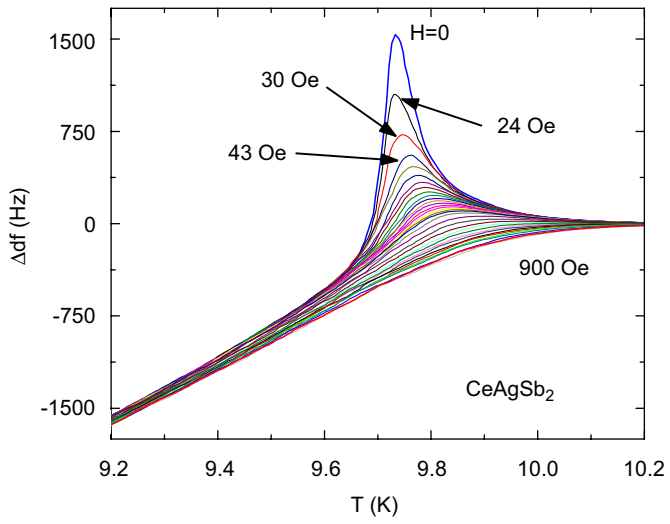

Fig. 7. (Color online) Suppression of peak in susceptibility in the vicinity of the ferromagnetic phase transition with applied magnetic field for $CeAgSb_2$. The data, unlike others presented in this work, are unshifted.

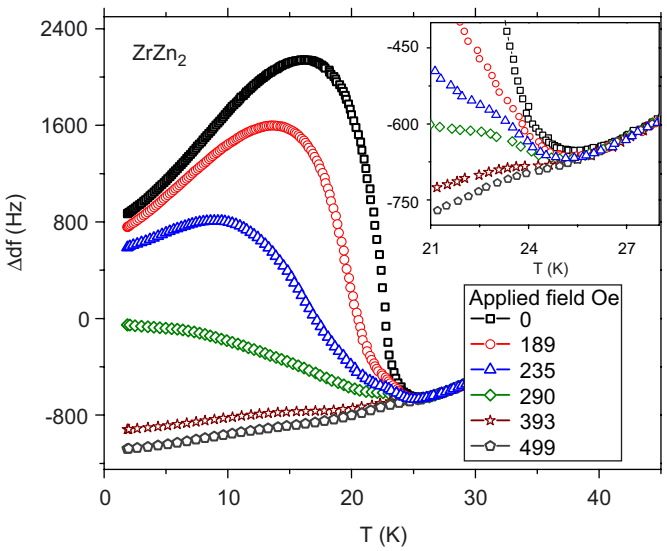

Fig. 8. (Color online) Change in resonant frequency in response to the itinerant ferromagnet $ZrZn_2$ in various magnetic fields. Inset: Detail of response near T_C.

affect the appearance of the peak at T_C. Therefore, it seems unlikely that demagnetization is responsible for the disappearance of the peak when the sample is oriented such that H_{exc} is perpendicular to the easy axis; rather it seems the TDO is sensitive to the magnetic anisotropy of the sample.

Fig. 7 shows magnetic susceptibility of the $CeAgSb_2$ in applied dc magnetic field. Weak applied fields suppress the peak dramatically and cause it to shift to higher temperatures. For fields up to 900 Oe the resonator response far from the peak is independent of the applied field. This is not surprising as the applied fields are too small for magnetoresistance to play a significant role. Indeed, reported magnetoresistance for this compound in the vicinity of the phase transition shows less than 5% change in ρ for fields up to about 1 kOe [14] and our own measurements show no detectable change if ρ in this field range. Also, it is evident from the data that there is little significant effect on the resonator response due to the applied field by about 9.4 K for the region below T_C and by about 10.2 K for the region above T_C.

3.1.3. $ZrZn_2$

$ZrZn_2$ is one of the prototypical weak itinerant ferromagnets ($T_C \approx 28$ K) [18]. Unlike $CeVSb_3$ and $CeAgSb_2$, $ZrZn_2$ does not manifest a sharp peak in the resonator frequency shift at T_C. Rather, zero field data show a large increase in susceptibility over a temperature range of approximately 5 K, a broad maximum, and a slower decrease in susceptibility. At lower temperatures as the applied dc field increases the temperature of the initial upturn in susceptibility does not shift, however the broad maximum is shifted to lower temperatures and is suppressed in amplitude. By 500 Oe the maximum virtually disappears (Fig. 8). Also of note is the lack of a local maximum in the vicinity of the phase transition.

Such extreme field dependence well below the transition indicates high polarizability of the itinerant magnetic order and cannot be explained by the direct contribution of the Brillouin variable $\mu H/k_B T$, where much larger fields would be required and the peak would shift to higher temperatures. Instead, it could be due to magnetic domains, which would then be quite different in itinerant ferromagnets compared to the local-moment systems and should be very weakly pinned, if at all. In this case, lower temperatures would be required to create domains opposite to the applied field, thus resulting in the maximum shift to lower temperatures.

3.1.4. $GdFe_2Zn_{20}$

$GeFe_2Zn_{20}$ is interesting for the present work as it contains both 4f (local moment) and 3d (potentially itinerant) moment elements. This compound develops a spontaneous magnetization below approximately 86 K, primarily associated with the gadolinium ions. The conduction electron background is highly polarizable (YFe_2Zn_{20} being just below the Stoner limit [15]) and in the ordered state a 0.3 μ_B induced moment on the iron opposes the gadolinium local moment [15]. Fig. 9 shows the measured TDO response due to this compound. The inset shows a detail of the signal near the ordering temperature. The small local maximum close to T_C exhibits behavior consistent with local moment ferromagnetic ordering, i.e., suppression in amplitude and shifting to higher temperatures with applied field. It is believed that this feature is associated with the ordering of the gadolinium moments. The large feature on the main graph is reminiscent of $ZrZn_2$, and therefore, believed to be associated with itinerant moments or a band-like component associated with this relatively high ordering temperature. AC susceptibility measurements on Pd–Mn alloys

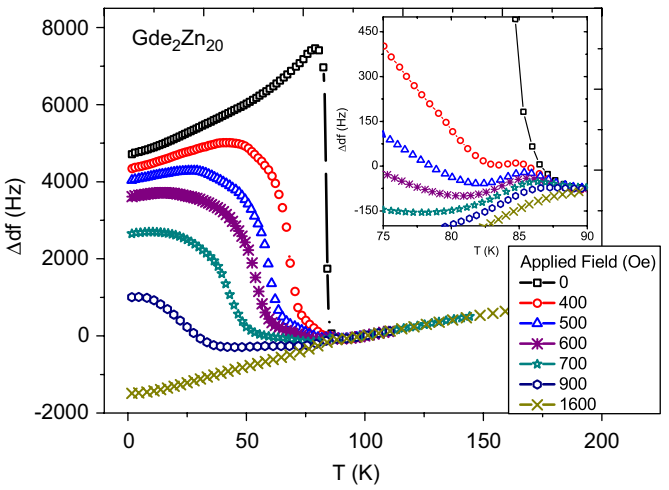

Fig. 9. (Color online) Variation of resonant frequency with temperature for $GdFe_2Zn_{20}$. Inset: Detail of response near T_C. The small peak is believed to be associated with the ordering of the localized gadolinium moments.

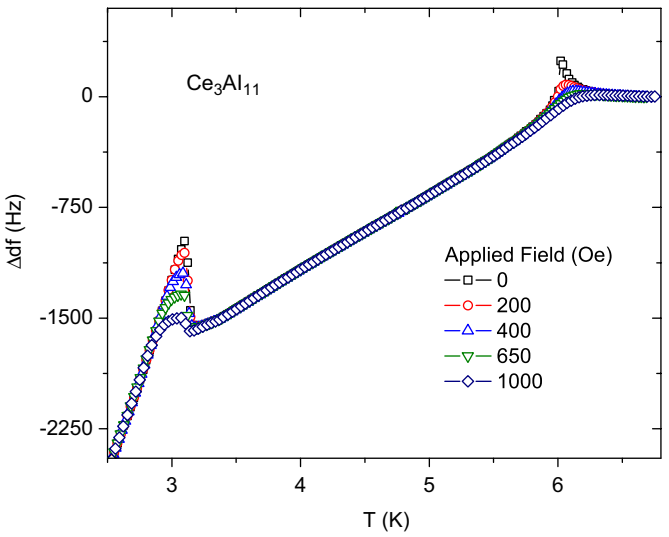

Fig. 10. (Color online) Response of oscillator to Ce_3Al_{11} in various magnetic fields through a ferromagnetic transition at 6 K and a transition to an incommensurate state at 3 K.

show strikingly similar behavior [25,26]. The data were interpreted as domain motion and measurement saturation associated with demagnetization effects. We believe the effect is from the separate responses of the polarization of the conduction electron subsystem. We note that a direct magneto-optical study of $CeAgSb_2$ (to be published elsewhere) shows very soft domains at low temperatures, yet they do not contribute to the low-temperature susceptibility as evident from Fig. 7. This means, if itinerant domains are responsible for the broad maximum in $\chi(T)$ in $GdFe_2Zn_{20}$ below T_C, they must be very different from domains formed by local moments. A study of this question is ongoing, including the construction of a new TDO to measure the transitions in nickel, iron and other higher T_C samples. Magneto-optical techniques will also be used for direct observations of the magnetic structure.

4. Multiple zero field and metamagnetic transitions

We now discuss two other compounds (Ce_3Al_{11} and CeSb), where the TDO was successfully used to measure changes in spin order as well as metamagnetic phase transitions.

4.1. Ce_3Al_{11}

The metallic compound Ce_3Al_{11} has a ferromagnetic transition at 6.2 K. Further cooling reveals another transition at 3.2 K to an incommensurate spin state. In the FM state there are two distinct cerium sites carrying different moments. The Ce_I site carries a moment of 1.27 μ_B while the Ce_{II} site carries a moment of 0.24 μ_B as described by Boucherle et al. [17]. TDO measurements clearly detect both transitions as shown in Fig. 10. The para- to ferro-transition is characterized by the familiar

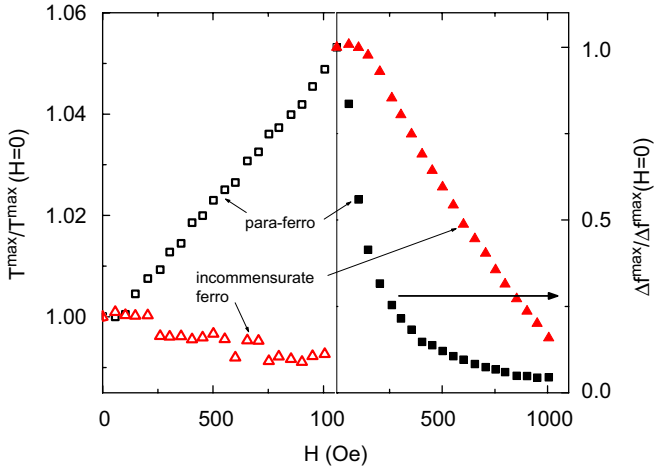

Fig. 11. (Color online) Normalized temperature (open symbols, left axis) and normalized amplitude (closed symbols, right axis) of susceptibility maxima near the two phase transitions of Ce_3Al_{11} relative to zero field temperatures. Squares denote PM to FM transition while triangles denote FM to incommensurate state transition.

sharp, asymmetric peak that suppresses in amplitude and shifts to higher temperatures with increasing applied field. The transition to the incommensurate state is marked by a rapid increase in the susceptibility followed by a decay as temperature continues to drop (Fig. 10). Application of magnetic field does not induce a significant temperature shift in this lower transition (Fig. 11), however it does trend slightly to lower temperatures, and the amplitude of the susceptibility increase is suppressed. It should be noted that far from the transitions, the measured signal is insensitive to applied fields, which means it is likely that the differences in response from one field to another we see are due only to the magnetic and not the skin effect component of χ.

The resistivity of Ce_3Al_{11} varies from 20 μΩ cm at 7 K to 5 μΩ cm at 2.5 K. Published data show that the resistivity is nearly constant from 7 K down to the FM transition where it exhibits a steep drop. Further, there is a change in slope in the resistivity versus temperature at the transition to the incommensurate state [27]. This corresponds to a skin depth at our operating frequency variation of approximately 68 μm at 7 K to 33 μm at 2.5 K. The sample used in this experiment had dimensions perpendicular to the excitation field approximately six times larger than the largest skin depth. Therefore, the TDO should be sensitive to the changes in ρ over temperature range of interest. This is consistent with the results presented here.

4.2. CeSb

Given that the TDO seems to be sensitive to multiple transitions, we decided to test this sensitivity with the binary compound CeSb, which has an extremely rich H–T phase diagram with many different ordered phases [11]. Each phase transition has an associated change in the long range magnetic order which is evident (to varying degrees) in thermodynamic and transport measurements. The changes in χ are readily seen in the raw data from the TDO (Fig. 12). It should be noted that TDO data alone will not, in general, give the actual ordering (e.g. FM vs. AFM) of any particular phase. Its use lies in its ability to detect phase change temperatures with extreme sensitivity. Temperature sweeps from 1.5 to 20 K were performed in 25 different applied fields ranging from 0–7.5 T. Temperatures of the peaks of the derivatives of the frequency shift were recorded for each field. The generated H–T phase boundary plot (Fig. 13) matches that from a combination of resistivity and magnetization measurements reported in

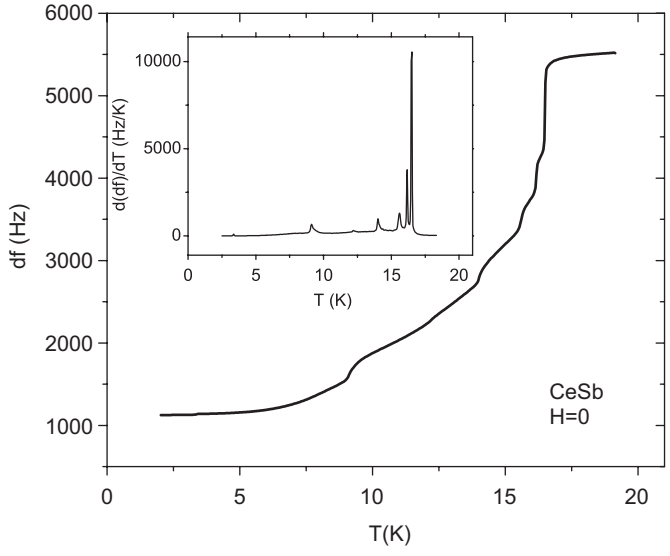

Fig. 12. Zero field response due to various magnetic transitions in CeSb. Inset: Derivative plot of main graph. The small peak at ~1.8 K is due to the suppressed superconducting transition of a small amount of tin flux residue from the crystal growth process.

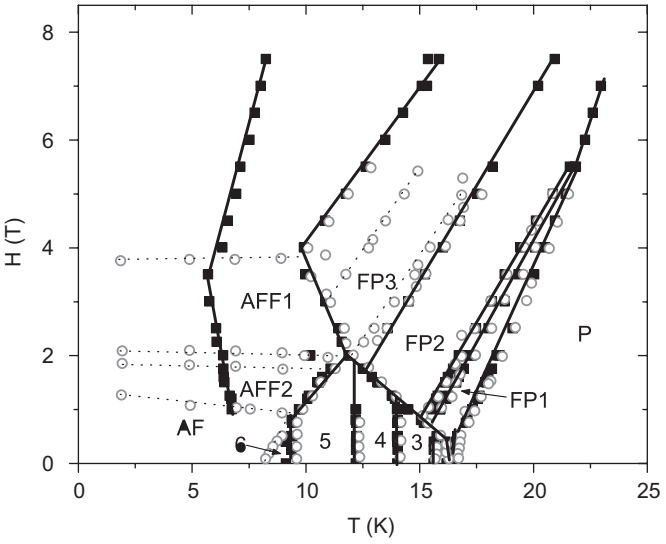

Fig. 13. H–T phase boundary plot for CeSb obtained from TDO response. Solid squares are this work, open circles are from Wiener and Canfield [11]. Solid lines represent phase boundaries determined by TDO measurements. Dotted lines are those boundaries missed by the TDO. Phases are labeled according to Ref. [11]. The low field AFM phases are denoted by numbers 3–6 from high temperature to low. The boundary between AFM1 and AFM2 is seen with the TDO, but not distinguishable on this scale.

Ref. [11] very well. Noticeably absent are the field induced transitions near 1, 2, and 4 T previously reported. In the present work no field sweeps at constant temperature were taken, so this is not surprising. It is likely that these boundaries would be seen by a TDO under the proper experimental procedures. Two other differences between this work and previous studies is here we measure a boundary that lies between 5 and 7 K for fields between 1 and 7.5 T, and we do not see the transition between two different ferro/para mixed states running along a line from about 12 K, 3 T to about 15 K, 5 T. The latter difference may be due to a chance perpendicular alignment of the ferromagnetic easy axis with respect to the excitation field as data were collected for only one orientation of the sample.

5. Scaling analysis of magnetic susceptibility

Finally, to demonstrate quantitative analysis capabilities, we present initial scaling analysis of our $CeVSb_3$ TDO data.

In the vicinity of a phase transition the correlation length over which local order exists diverges. This leads to the variation of thermodynamic quantities (e.g. specific heat or magnetic susceptibility) being dominated by power law behavior in either temperature or field. The field and temperature region over which this happens is the critical region, and the exponents are critical exponents or critical indices. Relevant for magnetic susceptibility measurements are the exponents β, δ, and γ defined by

$$m \sim t^{\beta}, \tag{10}$$

$$m \sim h^{1/\delta}, \tag{11}$$

$$\chi \sim t^{-\gamma}. \tag{12}$$

Here t is the reduced temperature and h is the reduced field.

$$t = 1 - \frac{T}{T_C}, \tag{13}$$

$$h = \frac{\mu H}{k_B T_C}. \tag{14}$$

In both of the above expressions T_C is defined as the zero field temperature of the phase transition and m is the magnetization per unit volume. The magnetic moment per ion is μ and k_B is the Boltzmann constant. It is straightforward to show that

$$\chi \sim h^{(1/\delta)-1}. \tag{15}$$

Analysis of critical phenomena rely on the assumption that the power law behavior completely dominates the system as the transition temperature is approached from below or above. The static scaling hypothesis requires that the free energy is a generalized homogeneous function in two variables, $F(t,h)$. Within scaling analysis it is enough to know the power law dependence of the free energy on temperature and field without knowing the actual form of the equation. This leads to the conclusion that only two of the critical-point exponents need to be determined. All others are derivable from various scaling relations. Further, under the static scaling hypothesis the exponents below T_C are equal to those above. Under the scaling hypothesis, the exponents β, δ, and γ are related by the following equation:

$$\gamma = \beta(\delta - 1), \tag{16}$$

from which we also find

$$\beta\delta = \beta + \gamma. \tag{17}$$

The above relations are based on the magnetic equation of state

$$m(h,t) = t^{\beta} G(h/t^{(\beta\delta)}), \tag{18}$$

where $G(h/t^{(\beta\delta)})$ is the first derivative of the free energy with respect to field. Differentiating with respect to h gives the susceptibility equation

$$\chi(h,t) = t^{-\gamma} \dot{G}(h/t^{(\beta\delta)}). \tag{19}$$

Measurements of susceptibility in various fields near T_C should fall on a common curve if plotted as $t^{\gamma}\chi$ versus $h/t^{\beta\delta}$ (Fig. 14). The value of γ can be estimated by fitting a line to a log–log plot of the TDO response vs. reduced temperature near T_C. Even though our system has an unknown offset in χ, the response should be dominated by the diverging component related to the phase transition. The resulting value of γ from our data is 1.4. The product $\beta\delta$ can be treated as an adjustable parameter. We find $\beta\delta = 1.34$ results in a good collapse of the data. While the value of γ is consistent with a 3D Heisenberg model, the product $\beta\delta$ is closer to the prediction of a 3D Ising model.

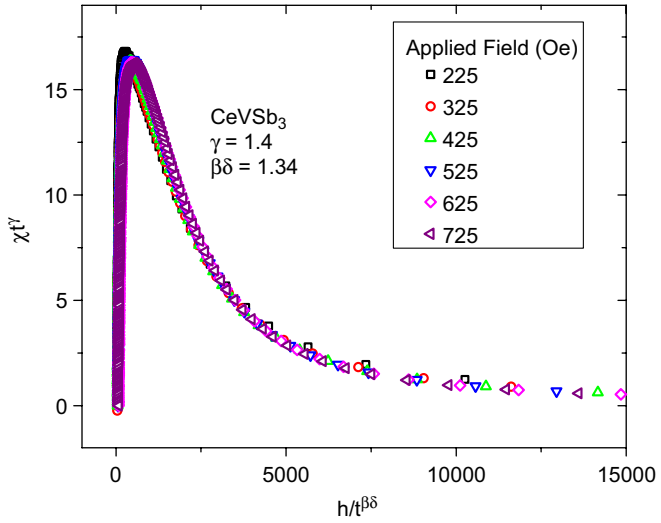

Fig. 14. (Color online) Plot of scaled susceptibility vs. scaled field for $CeVSb_3$. The temperature range shown is from 12 to 4.6 K left to right.

6. Conclusions

Sensitive TDO techniques were used to study magnetic susceptibility in several intermetallic magnetic compounds. It is demonstrated that the TDO has strong potential as an instrument with which to study magnetic phase transitions. Ferromagnetic transitions are of particular interest as the behavior of the susceptibility peak in the vicinity of T_C is largely inaccessible by other means. Low frequency ac susceptibility measurements do detect this peak, however the response is broadened in temperature and suppressed in amplitude relative to TDO measurements at comparable dc bias fields. The anisotropic response seems to allow one to measure the ferromagnetic easy axis of a compound in the zero field limit near T_C. The possibility to detect the difference in the dynamic response between weak itinerant and local moment magnets is very encouraging, because it is often difficult to determine the mechanism of magnetism in the ordered state. Quantitative analysis of the response was demonstrated for critical scaling near T_C.

Acknowledgments

Work at the Ames Laboratory was supported by the Department of Energy—Basic Energy Sciences under Contract No. DE-AC02-07CH11358. R.P. is grateful to his cat, Linux, for her purry support and acknowledges support from the NSF Grant no. DMR-06-03841 and the Alfred P. Sloan Foundation.

References

[1] R.B. Clover, W.P. Wolf, Rev. Sci. Instr. 41 (1970) 617.
[2] C.T.V. Degrift, Rev. Sci. Instr. 48 (1975) 599.
[3] F. Habbal, G.E. Watson, P.R. Elliston, Rev. Sci. Instr. 46 (1975) 192.

[4] R. Prozorov, R.W. Giannetta, Supercond. Sci. Technol. 19 (2006) R41.
[5] R. Prozorov, M.D. Vannette, G.D. Samolyuk, S.A. Law, S.L. Bud'ko, P.C. Canfield, Phys. Rev. B 75 (2007) 014413.
[6] J.N. Fox, N. Gaggini, J.K. Eddy, Am. J. Phys. 54 (1986) 723.
[7] P.V. Parimi, H. Srikanth, M. Bailleul, S. Sridhar, R. Suryanarayanan, L. Pinsard, A. Revcolevschi, cond-mat/0007377.
[8] G.T. Woods, P. Poddar, H. Srikanth, Y.M. Mukovskii, J. Appl. Phys. 97 (2005) 10C104.
[9] P.C. Canfield, I.R. Fisher, J. Cryst. Growth 225 (2001) 155.
[10] P.C. Canfield, Z. Fisk, Phil. Mag. B (1992) 65.
[11] T.A. Wiener, P.C. Canfield, J. Alloys Compd. 303–304 (2000) 505.
[12] A.S. Sefat, S.L. Bud'ko, P.C. Canfield, submitted for publication.
[13] K.D. Myers, S.L. Bud'ko, V.P. Antropov, B.N. Harmon, P.C. Canfield, Phys. Rev. B 60 (1999) 13371.
[14] K.D. Myers, S.L. Bud'ko, I.R. Fisher, Z. Islam, H. Kleinke, A.H. Lacerda, P.C. Canfield, J. Magn. Magn. Mater. 205 (1999) 27.
[15] S. Jia, S.L. Bud'ko, G.D. Samolyuk, P.C. Canfield, cond-mat/0606615.
[16] P.D. de Réotier, G. Lapertot, A. Yaouanc, P.C.M. Gubbens, S. Sakarya, A. Amato, Phys. Lett. A 349 (2006) 513.
[17] J.X. Boucherle, F. Givord, G. Lapertot, A.M. noz, J. Schweizer, J. Magn. Magn. Mater. 148 (1995) 397.
[18] E.A. Yelland, S.J.C. Yates, O. Taylor, A. Griffiths, S.M. Hayden, A. Carrington, Phys. Rev. B 72 (2005) 184436.
[19] A. Carrington, R.W. Giannetta, J.T. Kim, J. Giapintzakis, Phys. Rev. B 59 (1999) R14173.
[20] R. Prozorov, R.W. Giannetta, A. Carrington, F.M. Araujo-Moreira, Phys. Rev. B 62 (2000) 115.
[21] W.N. Hardy, D.A. Bonn, D.C. Morgan, R. Liang, K. Zhang, Phys. Rev. Lett. 70 (1993) 3999.
[22] J.D. Jackson, Classical Electrodynamics, Wiley, New York, 1998.
[23] D. Drobac, J. Magn. Magn. Mater. 159 (1996) 159.
[24] D. Drobac, J. Magn. Magn. Mater. 183 (1998) 71.
[25] S.C. Ho, I. Maartense, G. Williams, J. Phys. F 11 (1981) 699.
[26] S.C. Ho, I. Maartense, G. Williams, J. Phys. F 11 (1981) 1107.
[27] T. Ebihara, Y. Uwatoko, N. Mohri, J. Magn. Magn. Mater. 272–276 (2004) e83.